Available online at www.eccomasproceedia.org
Eccomas Proceedia COMPDYN (2025) 2472-2482

ECCOMAS
Proceedia

COMPDYN 2025
10th ECCOMAS Thematic Conference on
Computational Methods in Structural Dynamics and Earthquake Engineering
M. Papadrakakis, M. Fragiadakis (eds.)
Rhodes Island, Greece, 15-18 June 2025

A NOVEL 3D MACROELEMENT FOR THE SEISMIC ANALYSIS OF MASONRY STRUCTURES WITH EQUIVALENT-FRAME MODELS

C. Salvatori[1], G. Guerrini[1], A. Galasco[1] and A. Penna[1]

[1] Department of Civil Engineering and Architecture
University of Pavia
Via Ferrata, 3 – 27100 Pavia – Italy
{christian.salvatori, gabriele.guerrini, alessandro.galasco, andrea.penna}@unipv.it

Abstract

The seismic vulnerability of unreinforced masonry (URM) structures and their extensive presence worldwide has driven significant efforts in the assessment and retrofit of existing buildings and in the design and detailing of new construction. The seismic performance of existing URM buildings is often compromised by local overturning mechanisms, as they were predominantly conceived without consideration of horizontal forces. However, even if local failure is prevented through structural interventions or adequate construction details, the out-of-plane excitation may reduce the capacity of masonry walls to withstand the in-plane seismic demand. This paper presents a novel three-dimensional equivalent-frame macroelement that effectively couples the in-plane and out-of-plane responses of masonry walls under lateral loads. The proposed model extends a preexisting two-dimensional formulation, resorting to a computationally efficient axial-flexural integration to simulate the nonlinear behavior of URM panels with a limited number of degrees of freedom. Furthermore, a straightforward methodology to account for second-order geometrical effects is reported. The capability of the resulting macroelement formulation in reproducing lateral strength and stiffness, hysteretic cycles, and displacement capacity of masonry panels, is finally validated against experimental results.

Keywords: Nonlinear three-dimensional macroelement, out-of-plane response, equivalent-frame modeling, masonry structures, seismic analysis.

doi: 10.7712/120125.12582.25387

1 INTRODUCTION

Unreinforced masonry (URM) structures are among the most vulnerable building typologies when subjected to seismic events. Consequently, their widespread presence and architectural importance have driven considerable interest in developing efficient and effective modeling strategies for the seismic assessment of the existing building stock.

Finite [1] or discrete [2] element methods provide the most accurate and versatile solutions to reproduce the heterogeneity and the nonlinear response of masonry material. However, their computational cost generally restricts the field of applications to structural subsystems. In contrast, the more simplified equivalent-frame modeling (EFM) strategy balances accuracy with computational efficiency, making it the most employed approach for ordinary engineering practice. Indeed, this methodology deviates the focus from the local response of masonry material to the average behavior of entire masonry panels. In this context, resisting walls are discretized in nonlinear macroelements connected through rigid nodes, following a fictitious frame layout [3, 4]. EFM has proven reliable for buildings with a regular opening layout and governed by a three-dimensional box-like response [5]. However, its accuracy may decrease as the structure deviates from the fictitious frame configuration or when the global response is compromised by masonry delamination or local out-of-plane failure mechanisms [6].

The two-node two-dimensional macroelement proposed by Penna et al. [7] and implemented in the software TREMURI [4] has been widely used for the static and dynamic analysis of URM structures. Over the years, this macroelement has undergone several revisions to address limitations and enhance capabilities [8, 9]. Nevertheless, its formulation has remained restricted to the in-plane response of masonry members. Indeed, a common assumption when adopting the EFM strategy is to neglect the out-of-plane strength and stiffness of the elements with respect to the global building response, relying instead on post-processing procedures based on limit analyses to assess the activation of local out-of-plane failure mechanisms. However, in-plane and out-of-plane responses are not uncoupled, and their interaction might affect the reliability of the results even when local out-of-plane failure mechanisms are substantially inhibited through adequate construction detailing.

This paper presents a novel two-node macroelement that, although preserving its kinematics, extends the formulation proposed by Penna et al. [7] to the three-dimensional space and introduces an additional mid-height interface to capture the correct axial-flexural stiffness of the member in the elastic regime without iterative algorithms. The nonlinear biaxial axial-flexural response is instead modeled through a stripe or full fiber discretization of the end- and mid-height interfaces, prioritizing computational efficiency and constitutive model versatility, respectively. Additionally, the kinematics of the macroelement allows a simplified but reliable representation of second-order geometrical effects without increasing the computational time. The capabilities of the proposed macroelement are validated against two quasi-static cyclic shear-compression tests on calcium silicate masonry piers, subjected to in-plane [10] and out-of-plane [11] loading, respectively.

2 THREE-DIMENSIONAL MACROELEMENT FORMULATION

The two-node three-dimensional macroelement described in this paper builds upon the two-dimensional proposal of Penna et al. [7]. In fact, its completely mechanics-based formulation and its ability to describe the coupled axial-flexural response with a limited number of degrees of freedom proved effective and efficient for the static and dynamic analysis of unreinforced masonry (URM) structures. Moreover, the peculiar arrangement of the degrees of freedom enables decoupling between shear and flexural kinematics, while enforcing equilibrium at the element level through internal degrees of freedom.

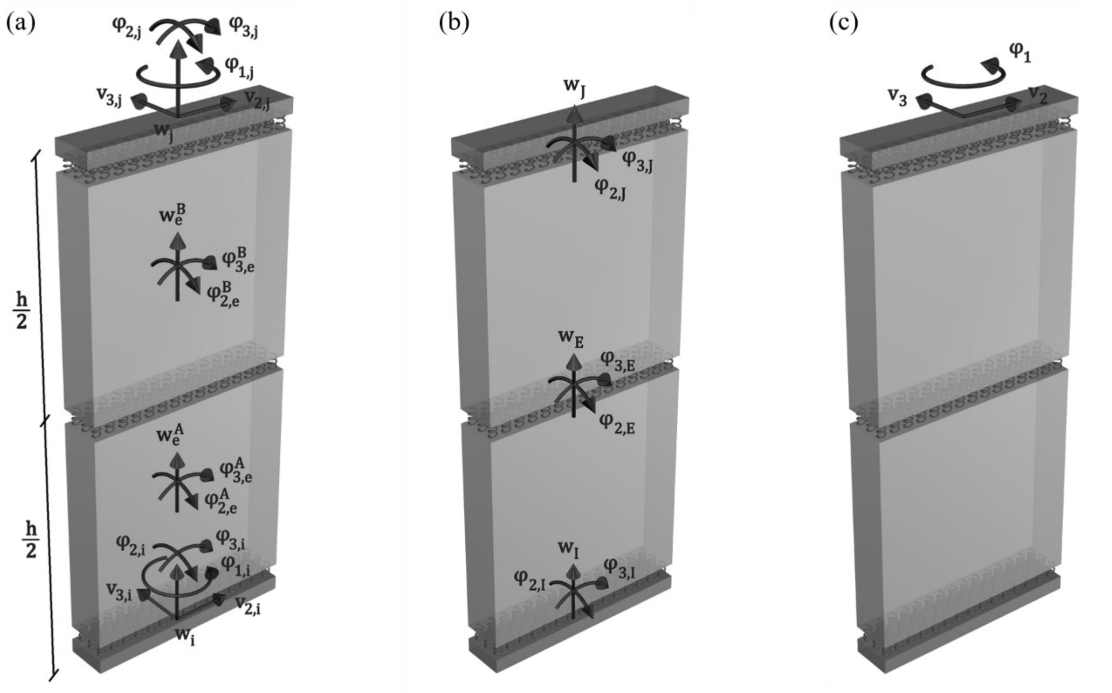

Figure 1: (a) Local degrees of freedom of the three-dimensional macroelement with the associated (b) interfaces and (c) central bodies basic generalized displacements.

Similarly to the formulation of Penna et al. [7], the proposed macroelement consists of interfaces separated by central bodies, accommodating the biaxial axial-flexural behavior on the one hand, and the shear and torsional responses on the other hand. However, unlike the original formulation, which includes only two end-interfaces, the novel macroelement introduces an additional mid-height interface that releases its kinematics and allows capturing the correct axial-flexural stiffness in the elastic regime, without requiring the iterative algorithm proposed by Bracchi et al. [8]. Indeed, the interfaces of the macroelement act as integration points that, according to the Gauss-Lobatto quadrature scheme, provide the exact solution of an elastic beam subjected to concentrated or uniformly distributed loads [12].

Overall, the kinematics of the macroelement is defined by eighteen local degrees of freedom (DOFs): displacements and rotations in three-dimensional space are assigned to each extremity and interact with external elements, while a vertical displacement and in-plane and out-of-plane rotations are introduced within the two central bodies as internal DOFs (Figure 1a). Starting from the local DOFs, the corresponding basic generalized displacements associated to the interfaces (Figure 1b) and central bodies (Figure 1c) are derived according to equations (1) and (2), respectively:

$$\begin{bmatrix} w_I \\ \varphi_{2,I} \\ \varphi_{3,I} \end{bmatrix} = \begin{bmatrix} w_e^A - w_i \\ \varphi_{2,e}^A - \varphi_{2,i} \\ \varphi_{3,e}^A - \varphi_{3,i} \end{bmatrix} \qquad \begin{bmatrix} w_E \\ \varphi_{2,E} \\ \varphi_{3,E} \end{bmatrix} = \begin{bmatrix} w_e^B - w_e^A \\ \varphi_{2,e}^B - \varphi_{2,e}^A \\ \varphi_{3,e}^B - \varphi_{3,e}^A \end{bmatrix} \qquad \begin{bmatrix} w_J \\ \varphi_{2,J} \\ \varphi_{3,J} \end{bmatrix} = \begin{bmatrix} w_j - w_e^B \\ \varphi_{2,j} - \varphi_{2,e}^B \\ \varphi_{3,j} - \varphi_{3,e}^B \end{bmatrix} \tag{1}$$

$$\begin{bmatrix} v_2 \\ v_3 \\ \varphi_1 \end{bmatrix} = \begin{bmatrix} v_{2,j} - v_{2,i} - \left(\varphi_{e,3}^A + \varphi_{e,3}^B\right)\frac{h}{2} \\ v_{3,j} - v_{3,i} + \left(\varphi_{e,2}^A + \varphi_{e,2}^B\right)\frac{h}{2} \\ \varphi_{1,j} - \varphi_{1,i} \end{bmatrix} \tag{2}$$

where h indicates the total height of the element.

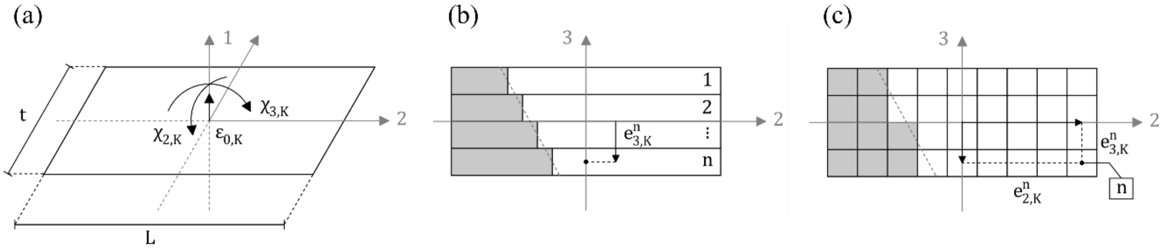

Figure 2: (a) Interface degrees of freedom, (b) stripe and (c) full fiber discretization of the cross-section.

Subsequently, the axial deformation ($\varepsilon_{0,K}$) and the in-plane ($\chi_{2,K}$) and out-of-plane ($\chi_{2,K}$) curvatures related to the K^{th} interface, are obtained through the basic genderized displacements as follows (Figure 2a):

$$\begin{bmatrix} \varepsilon_{0,K} \\ \chi_{2,K} \\ \chi_{3,K} \end{bmatrix} = \frac{1}{\tilde{w}_K h} \begin{bmatrix} w_K \\ \varphi_{2,K} \\ \varphi_{2,K} \end{bmatrix} \tag{3}$$

where $\tilde{w}_K$ represent the integration weights that, according to the Gauss-Lobatto integration scheme, are set to 1/6 and 2/3 by default for the end- and mid-height interfaces, respectively; however, different values can be assigned.

The biaxial flexural response of the macroelement is retrieved through a stripe (Figure 2b) or full fiber (Figure 2c) discretization of the interfaces. In the first case, a subdivision in n two-dimensional analytical stripes is performed, and the biaxial response is obtained by numerically integrating the contribution of each stripe along the out-of-plane direction of the macroelement [12]. In this context, the axial deformation ($\varepsilon^n_{0,K}$) and in-plane curvature ($\chi^n_{2,K}$) associated with the n^{th} stripe are derived according to equation (4):

$$\begin{cases} \varepsilon^n_{0,K} = \varepsilon_{0,K} + \chi_{2,K} e^n_{3,K} \\ \chi^n_K = \chi_{3,K} \end{cases} \tag{4}$$

where $e^n_{3,K}$ represents the out-of-plane eccentricity with respect to the centroid of the interface (Figure 2b).

As the contribution of each stripe is obtained through an analytical integration of the stresses along its length following the procedures described by Penna et al. [7], it results in a computationally efficient formulation. In this context, an elasto-fragile tensile strength accounts for cracking effects during rocking motions, whereas an elastic-perfectly plastic behavior in compression captures the limited compressive strength of masonry due to toe-crushing phenomena. Additionally, the cyclic response is modeled either using a recentering [7] (Figure 3a) or parallel-elastic [8] (Figure 3b) unloading branch. While the recentering response captures stiffness decay, the parallel-elastic unloading proved better at accounting for energy dissipation and residual displacements.

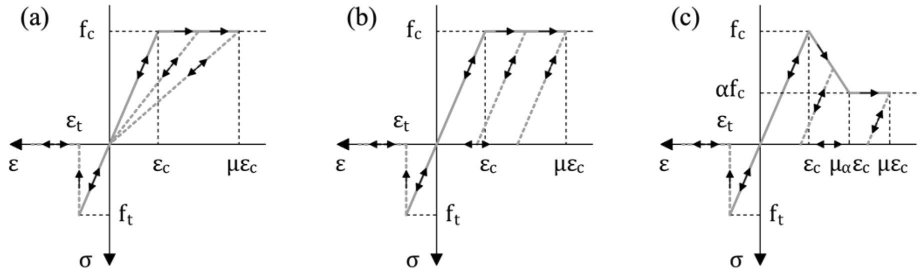

Figure 3: Interface constitutive laws: (a) Penna et al. [7], (b) Bracchi et al. [8], and (c) multilinear models.

Despite the computational advantages of the stripe formulation, the analytical integration restricts the applicability to simple constitutive laws. To overcome this limitation, the macroelement interfaces also provide a full fiber discretization, allowing more refined uniaxial stress-strain relationships. In this context, the multilinear model illustrated in Figure 3c adds to the constitutive laws previously described. However, this approach increases computational time, as the response of each fiber needs to be numerically integrated along the in-plane and out-of-plane directions of the cross-section. The uniaxial deformation of the n^{th} fiber is computed as follows:

$$\varepsilon_K^n = \varepsilon_{0,K} + \chi_{2,K} e_{3,K}^n - \chi_{3,K} e_{2,K}^n \tag{5}$$

where $e^n{}_{2,K}$ and $e^n{}_{3,K}$ indicate the in-plane and out-of-plane eccentricities with respect to the centroid of the interface (Figure 2c).

The shear and torsional responses of the macroelement are allocated in the central bodies and are considered independent among each other and along the two principal directions. More specifically, the first is governed by the Gambarotta and Lagomarsino continuum model for masonry [13, 14], adequately integrated to align with the macroelement formulation [7], while the second relies on a linear-elastic response, as generally of minor concern for masonry members. It is also worth pointing out that, in the current implementation, the macroelement considers nodal loads only. For this reason, the shear and torsional distortions have a constant profile and are computed by dividing the corresponding basic generalized displacements by the total height of the macroelement.

Starting from the basic generalized displacements reported in equations (1) and (2), the corresponding basic generalized forces are derived according to the constitutive laws outlined above, and are assembled into the vector of local forces to verify equilibrium:

$$\begin{bmatrix} N_i \\ V_{2,i} \\ V_{3,i} \\ M_{1,i} \\ M_{2,i} \\ M_{3,i} \end{bmatrix} = \begin{bmatrix} -N_I \\ -V_2 \\ -V_3 \\ -M_1 \\ -M_{2,I} \\ -M_{3,I} \end{bmatrix} \qquad \begin{bmatrix} N_j \\ V_{2,j} \\ V_{3,j} \\ M_{1,j} \\ M_{2,j} \\ M_{3,j} \end{bmatrix} = \begin{bmatrix} N_J \\ V_2 \\ V_3 \\ M_1 \\ M_{2,J} \\ M_{3,J} \end{bmatrix} \qquad \begin{bmatrix} N_e^A \\ M_{2,e}^A \\ M_{3,e}^A \\ N_e^B \\ M_{2,e}^B \\ M_{3,e}^B \end{bmatrix} = \begin{bmatrix} N_I - N_E \\ M_{2,I} - M_{2,E} + V_3 \frac{h}{2} \\ M_{3,I} - M_{3,E} - V_2 \frac{h}{2} \\ N_E - N_J \\ M_{2,E} - M_{2,J} + V_3 \frac{h}{2} \\ M_{3,E} - M_{3,J} - V_2 \frac{h}{2} \end{bmatrix} \tag{6}$$

Simplified second-order geometrical effects, which account for the interaction between axial force and lateral displacements, are incorporated into the macroelement formulation by resorting to its internal degrees of freedom [8]. Specifically, additional in-plane and out-of-plane bending moment contributions are assigned to the corresponding internal DOFs, according to equation (7):

$$\begin{bmatrix} M_{2,e}^A \\ M_{3,e}^A \\ M_{2,e}^B \\ M_{3,e}^B \end{bmatrix}_{P-\Delta} = \begin{bmatrix} M_{2,e}^A \\ M_{3,e}^A \\ M_{2,e}^B \\ M_{3,e}^B \end{bmatrix} + \begin{bmatrix} \frac{v_{3,j}-v_{3,i}}{2} + \left(\varphi_{2,e}^B - \varphi_{2,e}^A\right)\frac{h}{4} \\ \frac{v_{2,j}-v_{2,i}}{2} - \left(\varphi_{3,e}^B - \varphi_{3,e}^A\right)\frac{h}{4} \\ \frac{v_{3,j}-v_{3,i}}{2} - \left(\varphi_{2,e}^B - \varphi_{2,e}^A\right)\frac{h}{4} \\ \frac{v_{2,j}-v_{2,i}}{2} + \left(\varphi_{3,e}^B - \varphi_{3,e}^A\right)\frac{h}{4} \end{bmatrix} N_j \tag{7}$$

The additional contributions introduce unbalanced actions that are compensated by iteratively adjusting the macroelement generalized displacements until the internal actions associated with the internal DOFs vanish, ensuring equilibrium at the element level.

Although the described approach, commonly referred to as *P-Δ* effects, approximates more rigorous formulations, it proved to be sufficiently accurate for moderate displacements.

3 VALIDATION AGAINST EXPERIMENTAL RESULTS

The macroelement proposed in this paper is validated through the numerical simulation of the experimental response of two single-wythe calcium silicate (CS) masonry piers subjected to quasi-static cyclic shear-compression tests. More specifically, the first and the second specimens are tested along the in-plane and out-of-plane directions, respectively. The CS masonry piers are part of experimental campaigns conducted at the EUCENTRE Foundation and University of Pavia facilities in Italy [10, 11, 15].

3.1 Specimens and testing protocols

The in-plane (IP) shear-compression test were conducted on a CS masonry pier with dimensions 2.70×2.00×0.10 m, while the out-of-plane (OOP) specimen measured 2.70×1.10×0.10 m (Figure 4).

The mechanical properties of the masonry piers are derived from their respective characterization campaigns [10, 11, 15], involving bending and compression, bond-wrench, direct shear, and torsion tests, carried out at the DICAr Laboratory of the University of Pavia. The resulting Young's modulus (E), compressive and tensile strength of masonry (f_c, and f_t) and CS bricks (f_{bc} and f_{bt}), cohesion and friction coefficients (f_{v0} and μ), as well as the CS masonry density (ρ), are summarized in Table 1.

The cyclic shear-compression tests were performed by imposing increasing target displacements through a horizontal servo-hydraulic actuator, while two vertical actuators maintained a constant axial load and ensured double-curvature boundary conditions. More specifically, values corresponding to an average stress σ_0 of 0.5 MPa and 1.8 MPa were imposed at the top of the IP and OOP specimens, respectively. Also, a restraining system constrained the movement in the loading directions. The testing protocol of the IP specimen provided three cycles per displacement increment to investigate stiffness and strength degradation. On the other hand, no multiple repetitions were performed for the OOP specimen.

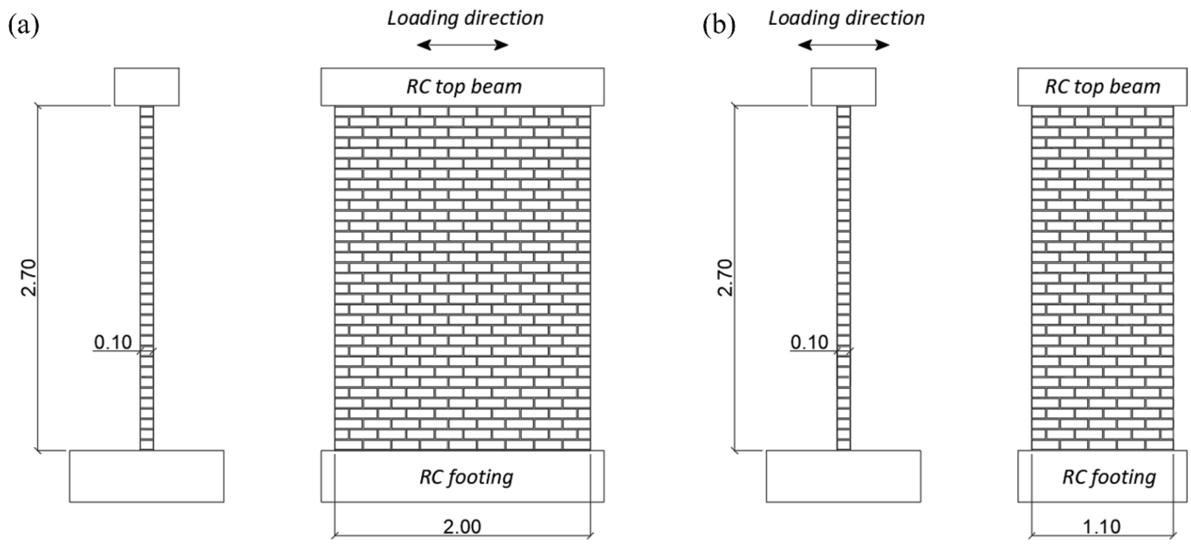

Figure 4: Experimental CS masonry piers: (a) IP and (b) OOP specimens.

[*] Estimates from the IP specimen characterization campaign.

	E [MPa]	G [MPa]	f_c [MPa]	f_t [MPa]	f_{v0} [MPa]	μ [-]	f_{bc} [MPa]	f_{bt} [MPa]	ρ [kg/m³]
IP specimen	6593	1978	10.1	0.28	0.62	0.71	19.8	2.50	1837
OOP specimen	6630	1989	10.1	0.40	0.62*	0.71*	19.8*	2.50*	1840

Table 1: Mechanical properties deduced from the characterization campaign of IP and OOP specimens.

3.2 Numerical modeling

The two CS masonry specimens are modeled with their actual dimensions, by imposing double-fixed boundary conditions. The mechanical properties assigned to the models totally reflect the outcomes of the two characterization campaigns, whose values are summarized in Table 1. Notably, only the compressive strength is reduced to 85% to account for the elastic-perfectly plastic idealization of the constitutive models reported in Figure 3a and Figure 3b, as the softening response cannot be reproduced. Conversely, the constitutive law of Figure 3c does not need any modification. In this context, a residual value of $\alpha f_c = 0.4 f_c$ is set at a deformation of $\mu_\alpha \varepsilon_c = 0.35\%$. Is it worth noticing that the shear modulus of masonry is assumed equal to $0.3E$, since no dedicated shear tests were conducted during the characterization campaigns.

The shear strength of the macroelement is modeled by assuming predefined failure criteria. The shear sliding ($V_{u,s}$) on the cracked length (L') and the stair-stepped diagonal cracking ($V_{u,d}$) are provided, consistently with the prescription of the Italian building code for masonry with regular texture [16, 17]:

$$\begin{cases} V_{u,s} = L'\, t\, f_{v0} + L\, t\, \mu\, \sigma_0 \leq f_{v0,lim}\, L'\, t \\ V_{u,d} = L\, t\, \left(\frac{f_{v0}}{1+\mu \tan\phi} + \frac{\mu}{1+\mu \tan\phi}\, \sigma_0\right) \leq \frac{L\,t}{2.3}\, f_{bt} \sqrt{1+\frac{\sigma_0}{f_{bt}}} \end{cases} \tag{8}$$

where $\varphi = 0.7$ represents the interlocking coefficient, function of the height and overlapping length of the units, whereas $f_{v0,lim}$ is a strength limitation due to the tensile failure of the CS bricks, which is typically expressed as a fraction of the corresponding compressive strength. Since characterization tests directly provide the tensile strength of bricks, $f_{v0,lim} = f_{bt}$ is assumed.

As previously reported, the shear response of the macroelement is governed by the Gambarotta and Lagomarsino model [13 ,14], whose nonlinear cyclic response is thoroughly defined by two parameters: Gc_t defines the position of the peak strength, whereas β described the slope of the post-peak softening branch. In particular, values of $Gc_t = 5$ and $\beta = 0.5$ are assumed.

The numerical analyses are carried out by subjecting the two piers to the corresponding experimental protocols, in both amplitude and number of cycles. Constant axial forces of 101.45 kN and 199.26 kN are assigned to the top of the IP and OOP numerical specimens, respectively, ensuring consistency with the average stresses imposed during the experimental tests.

3.3 Numerical results and comparison

Numerical results are compared to the experimental data focusing on hysteretic responses and failure mechanisms. Hysteresis cycles are presented in terms of drift ratios, namely the horizontal top displacements of the piers normalized to their heights, against the corresponding base shear restoring forces.

The numerical simulation of the IP specimen effectively replicates the failure mechanisms observed during the experimental test. Indeed, Figure 5 shows that both the numerical and experimental specimens exhibited a cracking-rocking response until reaching approximately 0.2% of drift ratio. Subsequently, the onset of a shear-sliding failure mechanism led to a sudden drop in strength at its permanent residual value.

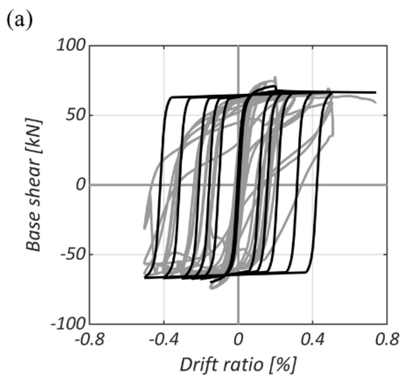

Figure 5: Hysteretic cycles of the IP specimen using the Penna et al. [7], Bracchi et al. [8], and (c) multilinear constitutive laws: (a) full load history, and (b) load history up to switching from rocking to shear-sliding failure mechanisms. Experimental and numerical responses in grey and black, respectively.

Elastic stiffness, lateral strength, and energy dissipation are in good agreement with the experimental outcomes, showing only marginal discrepancies of 5.5% and 3.9% for the peak and residual strength, respectively. It is worth noticing that the peak strength of the numerical model is governed by the limitation accounting for the tensile failure of the units ($f_{v0,lim}$), making the results highly sensitive to this parameter.

No influence is experienced from the constitutive law in compression adopted for the masonry material. In fact, the models reported in Figure 3 prove identical results, since the displacement history imposed does not lead to the attainment of the masonry compressive strength. Previous studies have also highlighted that the stripe and full fiber discretizations produce nearly overlapping results when using the material model from Figure 3a, with only minor discrepancies arising from the approximations inherent in the analytical integration procedure [18].

Also the numerical simulation of the OOP specimen provides results closely aligned to the experimental observations. Indeed, although approximated, the proposed procedure to model second-order geometrical effects successfully captured the reduction in lateral strength due to moderate displacements. It is worth noticing that, before comparing with the numerical outcomes, the experimental response has been corrected by removing the horizontal component induced by the axial force imposed by the vertical actuators. In fact, due to the moderate displacements at the top of the specimen, this applied force resulted slightly inclined from the vertical direction. While this caused a negligible variation in the vertical component, it led to a significant increase in horizontal forces, which needs to be properly accounted for.

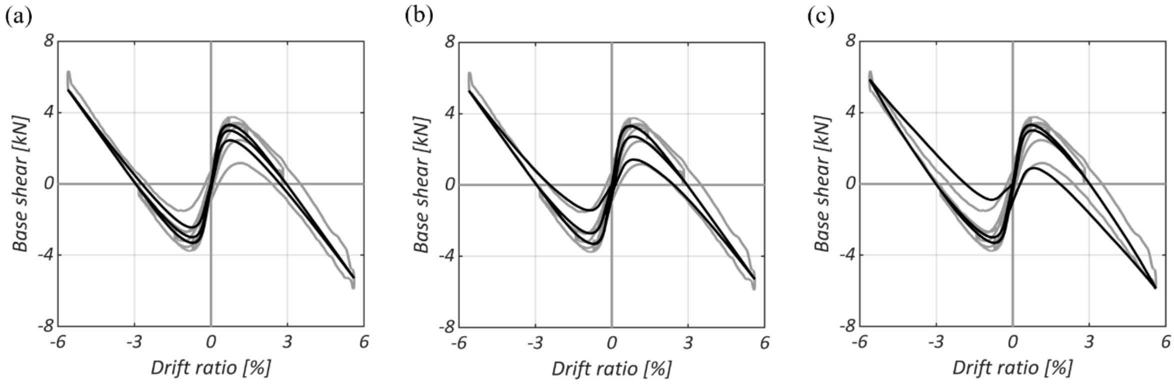

Figure 6: Hysteretic cycles of the OOP specimen using the (a) Penna et al. [7], (b) Bracchi et al. [8], and (c) multilinear constitutive laws. Experimental and numerical responses in grey and black, respectively.

Figure 6a, Figure 6b, and Figure 6c illustrate the numerical results obtained by adopting the masonry models reported in Figure 3a, Figure 3b, and Figure 3c, respectively. As shown, all constitutive laws satisfactorily capture the overall experimental trend. However, a notable discrepancy of 19% is observed for the peak strength, probably due to residual friction effects from the test set-up, given the very low lateral force capacity of the pier.

Nonetheless, the constitutive model proposed by Bracchi et al. (Figure 3b) accurately represents the cyclic response beyond the attainment of the compressive strength of masonry (Figure 6b). More specifically, the parallel-elastic unloading branch enhances the ability to account for damage accumulation and residual displacements compared to the recentering model of Figure 3a (Figure 6a). Furthermore, an additional benefit is given by the multilinear constitutive law of Figure 3c, whose softening response results in a more pronounced masonry plasticization, leading to an increased dissipated energy during cyclic loading (Figure 6c).

4 CONCLUSIONS

The equivalent-frame modeling (EFM) strategy is widely used for the seismic assessment of unreinforced masonry (URM) structures, offering a reasonable trade-off between accuracy of results and computational effort. This paper presents a novel three-dimensional equivalent-frame macroelement that overcomes certain limitations and extends the previous well-established two-dimensional formulation by incorporating the out-of-plane and torsional responses.

Through the introduction of an additional mid-height interface, the macroelement correctly reproduces the axial-flexural stiffness of a masonry panel without requiring iterative algorithms. Furthermore, a stripe or fiber discretization of the cross-section enables the modeling of the in-plane and out-of-plane axial-flexural interaction, balancing computational efficiency and constitutive law versatility.

The capabilities of the proposed macroelement are validated against two experimental quasi-static cyclic shear-compression tests on calcium silicate masonry piers, subjected to in-plane and out-of-plane loading, respectively. The mechanical properties assigned to the models directly reflect the outcomes of the corresponding experimental characterization campaigns.

The numerical model of the in-plane specimen shows good agreement with the experimental observations, satisfactorily reproducing elastic stiffness, lateral and residual strength, energy dissipation, and failure mechanisms. Since the model initially exhibits rocking behavior without toe-crushing, followed by a shear-sliding mechanism, the results show no influence of the axial-flexural constitutive law in compression assigned to the macroelement interfaces.

Also the model of the out-of-plane pier shows results satisfactorily aligned with the experimental counterpart. Indeed, the proposed formulation correctly captures second-order geometrical effects, proving a reduction in strength due to the influence of the axial load on horizontal displacements. Despite its simplicity, the parallel-elastic unloading of the elastic-perfectly plastic model enhances the cyclic axial-flexural response, providing a more accurate representation of energy dissipation and residual displacements compared to the recentering model. A further improved response is given by the more refined multilinear relationship, accommodating more pronounced masonry plasticization due to its softening branch.

Overall, the novel three-dimensional macroelement demonstrates its effectiveness in reproducing in-plane and out-of-plane responses of masonry elements, providing a trade-off between accuracy and computational effort also in case of moderate lateral displacements. Future developments will allow to further refine the formulation and to validate the macroelement against combined in-plane and out-of-plane static and dynamic tests.

ACKNOWLEDGEMENTS

This study is conducted within the DPC-ReLUIS (2024-2026) Work Package 10 “Code contributions for existing masonry constructions” funded by the Italian Department of Civil Protection (DPC). The authors would like to thank Nederlandse Aardolie Maatschappij BV (NAM) and the EUCENTRE Foundation, Italy, for funding and coordinating the experimental program. Note that the opinions and conclusions presented by the authors do not necessarily reflect those of the funding entities.

REFERENCES

[1] S. Degli Abbati, A.M. D’Altri, D. Ottonelli, G. Castellazzi, S. Cattari, S. de Miranda, S. Lagomarsino, Seismic assessment of interacting structural units in complex historic masonry constructions by nonlinear static analysis. *Computers and Structures*, **213**, 51-71, 2019.

[2] A.M. D’Altri, S. de Miranda, G. Castellazzi, V. Sarhosis, A 3D Detailed Micro-Model for the In-Plane and Out-Of-Plane Numerical Analysis of Masonry Panels. *Computers and structures*, **206**, 18–30, 2018.

[3] G. Magenes, A: Della Fontana, Simplified Non-Linear Seismic Analysis of Masonry Buildings. *Proceedings of the British Masonry Society*, **8**, 190-195, 1998.

[4] S. Lagomarsino, A. Penna, A. Galasco, S. Cattari, TREMURI Program: An Equivalent Frame Model for the Nonlinear Seismic Analysis of Masonry Buildings. *Engineering Structures*, **56**, 1787-1799, 2013.

[5] R. Siano, P. Roca, G. Camata, L. Pelà, V. Sepe, E. Spacone, M. Petracca, Numerical investigation of non-linear equivalent-frame models for regular masonry walls. *Engineering Structures*, **173**, 512-529, 2018.

[6] C. Morandini, D. Malomo, A. Penna, Equivalent Frame Discretisation for URM Façades with Irregular Opening Layouts. *Bulletin of Earthquake Engineering*, **20**(5), 2589-2618, 2022.

[7] A. Penna, S. Lagomarsino, A. Galasco. A Nonlinear Macroelement Model for the Seismic Analysis of Masonry Buildings. *Earthquake Engineering & Structural Dynamics*, **43**(2), 159-179, 2014.

[8] S. Bracchi, A. Galasco, A. Penna, A Novel Macroelement Model for the Nonlinear Analysis of Masonry Buildings. Part 1: Axial and Flexural Behavior. *Earthquake Engineering & Structural Dynamics*, **50**(8), 2233-2252, 2021.

[9] S. Bracchi, A. Penna, A Novel Macroelement Model for the Nonlinear Analysis of Masonry Buildings. Part 2: Shear Behavior. *Earthquake Engineering & Structural Dynamics*, **50**(8), 2212-2232, 2021.

[10] G. Guerrini, N. Damiani, M. Miglietta, F. Graziotti, Cyclic response of masonry piers retrofitted with timber frames and boards. *Proceedings of the Institution of Civil Engineers - Structures and Buildings*, **174**(5), 372–88, 2021.

[11] L. Grottoli, S. Kallioras, P. Korswagen, F. Graziotti, In-plane and out-of-plane quasi-static cyclic tests on unreinforced calcium-silicate masonry walls under high compressive load. *Research Report EUC067/2019U,* EUCENTRE Foundation, Pavia, Italy, 2019.

[12] F. Vanin, A. Penna, K. Beyer, A three-dimensional macroelement for modelling the in-plane and out-of-plane response of masonry walls. *Earthquake Engineering & Structural Dynamics*, **49**(14), 1365-1387, 2020.

[13] L. Gambarotta, S. Lagomarsino, Damage Models for the Seismic Response of Brick Masonry Shear Walls. Part I: The Mortar Joint Model and its Applications. *Earthquake Engineering & Structural Dynamics*, **26**(4), 423-439, 1997.

[14] L. Gambarotta, S. Lagomarsino, Damage Models for the Seismic Response of Brick Masonry Shear Walls. Part II: The Continuum Model and its Applications. *Earthquake Engineering & Structural Dynamics*, **26**(4), 441-462, 1997.

[15] F. Graziotti, A. Penna, G. Magenes, A comprehensive in situ and laboratory testing programme supporting seismic risk analysis of URM buildings subjected to induced earthquakes. *Bulletin of Earthquake Engineering*, **17**, 4575–4599, 2019.

[16] Ministry of Infrastructures and Transport, Norme Tecniche per le Costruzioni, DM 17/01/2018. *Ministry of Infrastructures and Transport*, Rome, Italy, 2018 (in Italian).

[17] Ministry of Infrastructures and Transport, Istruzioni per l'Applicazione dell'Aggiornamento delle "Norme Tecniche per le Costruzioni", Circ. 7 of 21/01/2019. *Ministry of Infrastructures and Transport*, Rome, Italy, 2019 (in Italian).

[18] C. Salvatori, G. Guerrini, A. Galasco, A. Penna, A Macroelement Formulation for Modeling Strengthened and Reinforced Masonry Elements. In: Milani, G., Ghiassi, B. (eds) *18th International Brick and Block Masonry Conference. IB2MaC 2024*. Lecture Notes in Civil Engineering, **613**. Springer, Cham, 2024.